PAPER • OPEN ACCESS

Extending the degree of polarization concept to higher-order and orbital angular momentum Poincaré spheres

To cite this article: David Marco *et al* 2022 *J. Opt.* **24** 124003

View the article online for updates and enhancements.

Extending the degree of polarization concept to higher-order and orbital angular momentum Poincaré spheres

David Marco[1,2] , **María Del Mar Sánchez-López**[1,3] , **Carlos Hernández-García**[4] and **Ignacio Moreno**[1,5,*]

[1] Instituto de Bioingeniería, Universidad Miguel Hernández de Elche, E-03202 Elche, Spain
[2] Aix Marseille Université, CNRS, Centrale Marseille, Institut Fresnel, UMR 7249, 13397 Marseille Cedex 20, France
[3] Departamento de Física Aplicada, Universidad Miguel Hernández de Elche, E-03202 Elche, Spain
[4] Grupo de Investigación en Aplicaciones del Láser y Fotónica, Departamento de Física Aplicada, Universidad de Salamanca, E-37008 Salamanca, Spain
[5] Departamento de Ciencia de Materiales, Óptica y Tecnología Electrónica, Universidad Miguel Hernández de Elche, 03202 Elche, Spain

E-mail: i.moreno@umh.es

CrossMark

Abstract
In this work, the density matrix formalism that describes any standard polarization state (fully or partially polarized) is applied to describe vector beams and spatial modes with orbital angular momentum (OAM). Within this framework, we provide a comprehensive description of the mapping between the corresponding Poincaré spheres (PSs); namely: the polarization PS, the higher-order PS (HOPS) and the orbital angular momentum PS (OAMPS). Whereas previous works focus on states located on the surface of these spheres, here we study vector and scalar modes lying inside the corresponding PS. We show that they can be obtained as the incoherent superposition of two orthogonal vector (or scalar) modes lying on the corresponding sphere surface. The degree of polarization (DoP) of a classical polarization state is thus extended to vector beams and OAM modes. Experimental results validate the theoretical physical interpretation, where we used a *q*-plate to map any state in the polarization PS onto the HOPS, and a linear polarizer to finally project onto the OAMPS. Three input states to such *q*-plate-polarizer system are considered: totally unpolarized, partially polarized, and fully polarized light. For that purpose, we design a new polarization state generator, based on two geometric phase gratings and a randomly polarized laser, which generates partially polarized light in an efficient and controlled way. We believe that the extension of the DoP concept to vector and OAM beams introduces a degree of freedom to describe spatially polarization and phase variant light beams.

(Some figures may appear in color only in the online journal)

---

* Author to whom any correspondence should be addressed.

1. Introduction

Scalar and vector beams carrying orbital angular momentum (OAM) have become a very popular field in Optics [1, 2]. The different techniques developed to generate these beams led to what is referred to nowadays as structured light [3]. These beams are finding applications in a myriad of areas, including imaging and microscopy [4], laser materials processing [5], optical trapping [6], classical and quantum optical communications [7] or quantum computing [8], to mention a few.

Different methods have been developed to produce beams with OAM. For instance, vortex beams carrying OAM have been generated with pairs of cylindrical lenses [9], holographic optical elements [10] or with spatial light modulators (SLMs) [11]. One simple practical device to generate and manipulate such beams is the q-plate, a geometric phase (GP) optical element that consists in a spatially patterned half-wave plate, made of liquid-crystal [12, 13] or of metamaterials [14], whose principal axis follows the azimuthal coordinate as $q\theta$. The topological singularity of charge q at the plate center typically takes integer or semi-integer values. This device, when illuminated with circularly fully polarized light, produces an output vortex beam with the opposite circular polarization state and helical phase $\pm 2q\theta$. While the spin angular momentum (SAM) of light is related to the polarization state, the OAM for these beams is associated with a spiral wavefront; beams with a spiral phase $\ell\theta$ carry an OAM of $\ell\hbar$ per photon. Hence, the q-plate induces an optical spin-to-OAM conversion.

The q-plate has also become very relevant to generate vector beams in a simple way [15, 16]. For instance, when illuminated with linearly fully polarized light it produces a linearly fully polarized output vector beam of cylindrical symmetry. These cylindrically polarized vector beams are the superposition of two scalar vortex beams with opposite OAM, each encoded onto one circular polarization state, thus leading to the maximum non-separability between the spatial mode and the polarization degrees of freedom [17].

A very useful geometrical representation of the polarization states and their transformation upon optical elements is the Poincaré sphere (PS) [18]. In this framework, the Stokes parameters, which fully describe a polarization state, are the Cartesian coordinates of a point in the sphere. Their longitude and the latitude coordinates are related, respectively, to the azimuth and the ellipticity of the polarization state. Hence, circularly polarized states are located on the poles of the PS, while linearly polarized states are on the equator. Any point on the PS can be obtained as a coherent superposition of right and left circularly polarized states.

The equivalent relations between the coherent superposition of polarization states and the coherent superposition of spatial modes led to the identification of the orbital angular momentum Poincaré sphere (OAMPS) [19]. In this sphere, first-order Laguerre–Gaussian (LG) modes with zero radial index of opposite OAM are located on the poles while the equator contains Hermite–Gaussian (HG) modes of different orientation. Although other beams carrying OAM can be represented in an OAM sphere [2], here we study the original

case of first-order LG and HG modes superposition [19]. Furthermore, a direct mapping between the polarization states on the PS and the modes on the OAMPS was identified [20]. This mapping connection between the 2D space of polarization represented by the PS and the 2D subspace of OAM can be physically realized very simply by means of a q-plate followed by a linear polarizer. Similarly, a higher-order Poincaré sphere (HOPS) was proposed to represent vector beams by extending the basis to the total optical angular momentum that includes the SAM and OAM [21]. In other words, the HOPS is the direct product space between the SAM and the OAM subspaces. Like in the OAMPS, the HOPS poles can be set to be Laguerre–Gaussian beams with opposite angular indices, but now with opposite circular polarization states. Therefore, their coherent superposition results in cylindrical vector beams. The equator corresponds to linearly polarized vector beams, while the intermediate points between the poles and equator correspond to elliptically polarized vector beams. Shortly afterwards, a hybrid-order PS was proposed, where the topological charges of the circularly polarized vortex modes of a vector beam can take any value [22], and different techniques have been proposed to their experimental realization [23, 24].

All these works consider only states located on the surface of the corresponding PS. However, in the classical PS, while states on the surface are fully polarized, states inside the sphere are partially polarized [18]. In fact, the distance from the center of the sphere is a measure of the well-known concept of degree of polarization (DoP), where the center of the PS corresponds to fully non-polarized light. The DoP is indeed a very relevant polarimetric parameter, for instance in biological applications [25, 26], an area where the use of structured polarization is being investigated to improve the sensing capability of polarimeter systems [27].

Since ideally a waveplate does not change the DoP of the input beam, we can envisage that illuminating a q-plate with partially polarized light will generate output vector modes with the same DoP as the input light, described by a point inside the HOPS, where its distance to the sphere center would give the DoP of the vector mode as a whole. This concept of the DoP of a vector beam can be interesting if we are to make polarimetry with these beams. Because of their polarization spatial pattern, vector beams have been proposed to develop snapshot polarimeters [28]. Also, generalized Stokes parameters based on cylindrical vector beams have been defined [21]. Hence, conventional polarimeter techniques (that use homogeneous polarization) could be extended to higher-order polarimetry, where the states involved in the illumination and detection are vector beams. In this context, it is essential to determine their DoP.

The concept of DoP presents particular relevance in the context of ultrafast laser pulses, emitted in the femtosecond or even attosecond regimes. In such cases, one can define an instantaneous DoP obtained through the Stokes parameters measured at a given temporal instant along the pulse. Though the instantaneous DoP is typically one, the polarization state or ellipticity might vary along the pulse, and thus the incoherently integrated DoP might reveal information of a partially polarized laser pulse. This interpretation can be also

performed in the spectral regime, where the frequency components of the laser pulse might present different polarization states, giving rise to a DoP different from one. This temporal variation of the polarization state of ultrafast laser pulses is particularly interesting in the context of high-order harmonic generation, where the time-dependent polarization state of the high-frequency pulses that are emitted provides information about the ultrafast laser-driven electron dynamics that take place in the generating medium [29–31]. During the last decade, vector beams have been also generated in the ultrafast regime. Triggered by the translation of the application of vector beams to ultrafast timescales, few-cycle infrared femtosecond vector beams have been generated [32]. In such cases, a complete spatiotemporal characterization of their polarization properties is possible thanks to the development of interferometric techniques [33]. But the extension of these techniques to higher frequency regimes, in order to completely characterize the spatiotemporal distribution of ultrafast extreme-ultraviolet vector beams [34, 35] is not trivial. In such scenarios, the characterization of the DoP of an ultrafast vector beam becomes relevant for their applications.

Thus, the goal of this work is to extend the classical DoP concept in the PS to the other PSs and to give a physical interpretation of the inner part of the OAMPS and the HOPS. For this purpose, we consider the incoherent superposition of two orthogonal polarization states on the surface of the PS to generate a partially polarized state, where the length p of the Stokes vector determines the classical DoP. This partially polarized beam is used as the input to a q-plate to generate a vector beam, and it is projected onto a polarizer to generate an OAM mode. We exploit the one-to-one mapping between the different PSs and we use the density matrix formalism to describe vector beams and spatial modes with OAM. This theoretical framework is presented in section 2. We show that the input DoP is maintained on the vector beam after the q-plate and that it can be regarded as an equivalent degree of purity of the superposition of pure modes on the OAMPS, here considered as the length of the Bloch vector of the simplest two-dimensional Bloch sphere [36, 37]. The examples are illustrated using the well-known Laguerre–Gaussian beams, although this formalism can be used to describe other beams with OAM.

Experimental results are presented that validate the theory. In section 3 we describe the experimental arrangement that we have developed to generate a light beam with variable DoP. It consists of a continuous laser with random polarization in combination with a compact polarization interferometer based on two GP gratings. This optical system bears advantages over other methods proposed to generate beams with controlled DoP that require either long paths [38], long temporal integrations [39] or spatial averaging [40]. The beam with controlled DoP is the input to a q-plate that maps any state in the polarization PS onto the HOPS, and it is finally projected onto the OAMPS through a linear polarizer. The experimental results are discussed in section 4, where three input beams of different DoP are sent to the q-plate. In each case, we analyze the properties of the output vector beam, as well as the properties of the projected scalar OAM mode, by using a polarimetric

approach combined with modal decomposition. Finally, in section 5 we point out the main conclusions of this work.

2. Theory

In this section, we first review the polarization matrix used to describe partially polarized light, its relation with the density operator for describing mixed states and with the classical PS, to later make use of the analogs in the HOPS and OAMPS. Figure 1 depicts the mapping between spheres through a q-plate-polarizer system. Figures 1(a)–(c) show, respectively, the PS, the HOPS and the OAMPS.

2.1. Polarization matrix and the density operator

The polarization properties of a spatially coherent paraxial light field with arbitrary DoP can be described by means of the polarization matrix [41] in terms of the correlations at time t between two orthogonal polarization components of complex amplitudes $E_i(t)$ and $E_j(t)$. The polarization matrix can be regarded as the matrix form of an operator:

$$
\begin{aligned}
\boldsymbol{\rho}_{\mathrm{P}} &= \rho_{ii}\,|i\rangle\langle i| + \rho_{jj}\,|j\rangle\langle j| + \rho_{ij}\,|i\rangle\langle j| + \rho_{ji}\,|j\rangle\langle i| \\
&= \begin{pmatrix} \rho_{ii} & \rho_{ij} \\ \rho_{ji} & \rho_{jj} \end{pmatrix},
\end{aligned}
\tag{1}
$$

where the vectors $|i\rangle$ and $|j\rangle$ are two orthogonal polarization components of complex amplitudes $E_i(t)$ and $E_j(t)$, respectively, and $\rho_{ij} = E_i^*(t)E_j(t)$. The brackets $\langle\,\rangle$ denote time averaging over the detection time. The diagonal elements ρ_{ii} and ρ_{jj} are auto-correlation functions at a given point of $E_i(t)$ and $E_j(t)$, respectively. ρ_{ii} and ρ_{jj} are positive quantities directly proportional to the irradiance for each polarization component i and j. The total field irradiance is proportional to $\rho_{ii} + \rho_{jj} = \mathrm{Tr}\boldsymbol{\rho}_{\mathrm{P}}$. Since the trace (Tr) is invariant under a change of basis, this value is also given by $\mathrm{Tr}\boldsymbol{\rho}_{\mathrm{P}} = \lambda_1 + \lambda_2$, where λ_1 and λ_2 are the eigenvalues of $\boldsymbol{\rho}_{\mathrm{P}}$. From now on, we will refer to the diagonal elements of the polarization matrix and its sum as intensities, following the usual nomenclature in the field [18].

On the other hand, the off-diagonal terms ρ_{ij} and ρ_{ji} are cross-correlation functions between $E_i(t)$ and $E_j(t)$ at a given point at the same time. The cross-correlation functions satisfy $\rho_{ji} = \rho_{ij}^*$, hence $\boldsymbol{\rho}_{\mathrm{P}}$ is a Hermitian matrix. The absolute value of the normalized quantity $\tilde{\rho}_{ij} = \rho_{ij}/\sqrt{\rho_{ii}\rho_{jj}}$ measures the correlation between $E_i(t)$ and $E_j(t)$, where $0 \leqslant |\tilde{\rho}_{ij}| \leqslant 1$. For $|\tilde{\rho}_{ij}| = 1$ the complex amplitudes $E_i(t)$ and $E_j(t)$ are perfectly correlated, while for $\tilde{\rho}_{ij} = 0$ there is no correlation between them. Intermediate values of $|\tilde{\rho}_{ij}|$ denote partial correlation.
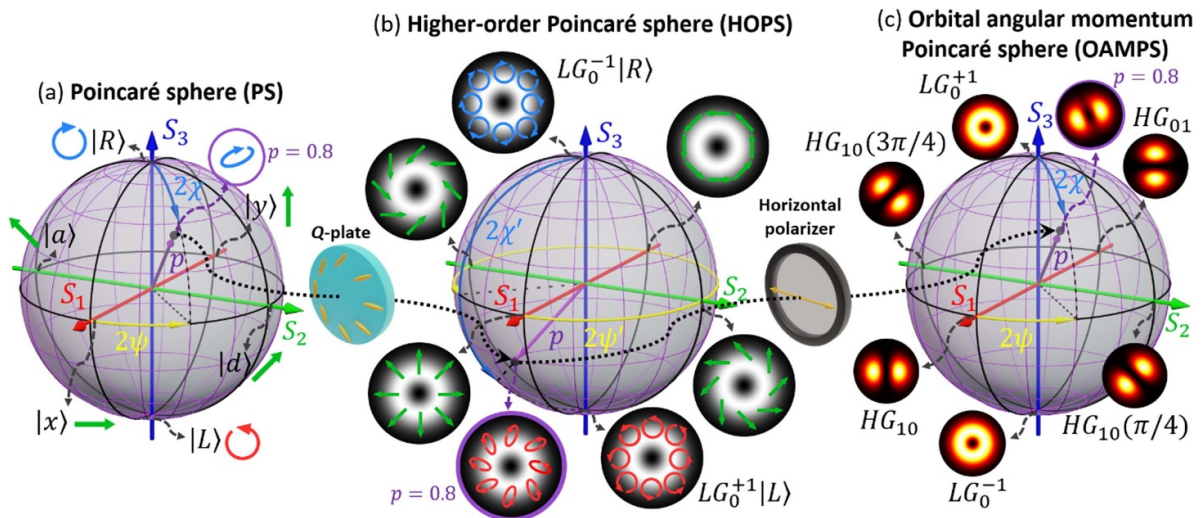
The DoP of the light described by $\boldsymbol{\rho}_{\mathrm{P}}$ is given by [41]:

$$
p = \sqrt{1 - \frac{4\,\mathrm{Det}\boldsymbol{\rho}_{\mathrm{P}}}{(\mathrm{Tr}\boldsymbol{\rho}_{\mathrm{P}})^2}} = \sqrt{1 - \frac{4\,\lambda_1\lambda_2}{(\lambda_1 + \lambda_2)^2}}\,.
\tag{2}
$$

The DoP is a positive quantity ranging from 0 to 1, where $p = 1$ stands for fully polarized light, $p = 0$ for unpolarized light and $0 < p < 1$ for partially polarized light.

Assuming a normalized beam intensity ($\mathrm{Tr}\boldsymbol{\rho}_{\mathrm{P}} = \rho_{ii} + \rho_{jj} = 1$) and fully uncorrelated $E_i(t)$ and $E_j(t)$ functions ($|\tilde{\rho}_{ij}| = 0$),

3

Figure 1. Conversion of a point in the (a) polarization Poincaré sphere to a point in the (b) HOPS through a $q = 1/2$ q-plate, and then to a point in the (c) OAMPS through a horizontal linear polarizer. Note that the beam has to be renormalized after the polarizer so that the last sphere is also of unit radius. Right (left)-handed polarization states are depicted in blue (red) and linear states are depicted in green. The polarization ellipses corresponding to partially polarized light in (a) and (b) describe the polarized part of the state, and they have been rescaled with the DoP.

the DoP is then given by $p = |2\rho_{ii} - 1|$. This situation describes an incoherent superposition of two beams in the polarization states $|i\rangle$ and $|j\rangle$, where the intensity of each component (ρ_{ii} and $\rho_{jj} = 1 - \rho_{ii}$) determines the DoP of the resulting beam. For $\rho_{ii} = 1$, the only component of the beam is in the polarization state $|i\rangle$, so the light is fully polarized ($p = 1$). On the other hand, the incoherent superposition of two equally-weighted polarization components ($\rho_{ii} = \rho_{jj} = 1/2$) yields unpolarized light ($p = 0$). The intermediate situation of partially polarized light ($0 < p < 1$) can be achieved by varying the weight of each component in the incoherent superposition. Let us note that since $|\tilde{\rho}_{ij}| = 0$ the off-diagonal terms in $\boldsymbol{\rho}_{\mathrm{P}}$ vanish. Consequently, $|i\rangle$ and $|j\rangle$ are the eigenstates of $\boldsymbol{\rho}_{\mathrm{P}}$, and ρ_{ii} and ρ_{jj} are directly its eigenvalues λ_1 and λ_2. In this work, we obtain partially polarized light in such a way, i.e. as an incoherent superposition of two fully polarized beams.

Let us remark that even if $|\tilde{\rho}_{ij}| \neq 0$ for a given basis $|i\rangle$ and $|j\rangle$, it is always possible to find an orthonormal basis of eigenstates $|e\rangle$ and $|e^{\perp}\rangle$ where $\boldsymbol{\rho}_{\mathrm{P}}$ is diagonal and therefore $|\tilde{\rho}_{ee^{\perp}}| = 0$. This means that partially polarized light can always be regarded as the incoherent superposition of two fully polarized states $|e\rangle$ and $|e^{\perp}\rangle$. The eigenvalues of $\boldsymbol{\rho}_{\mathrm{P}}$ are then the intensity of each polarization component, with $\lambda_1 = \rho_{ee}$ and $\lambda_2 = \rho_{e^{\perp}e^{\perp}}$. Considering normalized intensities and using equation (2) to get the eigenvalues as a function of the DoP, $\lambda_1 = \rho_{ee} = (1 + p)/2$ and $\lambda_2 = \rho_{e^{\perp}e^{\perp}} = (1 - p)/2$, the operator $\boldsymbol{\rho}_{\mathrm{P}}$ can be written in its eigenbasis as:

$$\boldsymbol{\rho}_{\mathrm{P}} = \frac{1+p}{2}|e\rangle\langle e| + \frac{1-p}{2}|e^{\perp}\rangle\langle e^{\perp}|. \tag{3}$$

Note that the above equation has the form of the density operator of a mixed state in quantum mechanics, which describes a probabilistic mixture of pure states $|e\rangle$ and $|e^{\perp}\rangle$ with probabilities $(1 \pm p)/2$. From the classical point of

view, it can be regarded as a description of an incoherent superposition of two orthogonal polarization states $|e\rangle$ and $|e^{\perp}\rangle$, where $(1 \pm p)/2$ are the intensities of the polarization components $|e\rangle$ and $|e^{\perp}\rangle$, respectively. For $p = 1$ (fully polarized light) the operator is $\boldsymbol{\rho}_{\mathrm{P}} = |e\rangle\langle e|$, which is a so-called pure state. For $p \neq 1$ (partially polarized light) it is said to be a mixed state. For $p = 0$ (unpolarized light), the operator is $\boldsymbol{\rho}_{\mathrm{P}} = (|e\rangle\langle e| + |e^{\perp}\rangle\langle e^{\perp}|)/2 = \boldsymbol{I}/2$, being $\boldsymbol{I} = |e\rangle\langle e| + |e^{\perp}\rangle\langle e^{\perp}|$ the identity operator. In this case, we have a maximally mixed state, which can be classically understood as an incoherent superposition of equally weighted orthogonal polarization components.

Alternatively, the last equation can be rewritten in terms of the identity operator as:

$$\boldsymbol{\rho}_{\mathrm{P}} = \frac{1-p}{2}\boldsymbol{I} + p|e\rangle\langle e|. \tag{4}$$

The first term in the sum stands for the unpolarized part of the beam, since it is the only remaining term for $p = 0$. On the other hand, the second term stands for the fully polarized part of the beam, since $\boldsymbol{\rho}_{\mathrm{P}} = |e\rangle\langle e|$ for $p = 1$.

2.2. Stokes parameters and the PS

An arbitrary fully polarized state $|e\rangle$ (henceforth called pure state) can be expressed as a coherent superposition of the right and left-circular polarization components ($|R\rangle$ and $|L\rangle$):

$$|e\rangle = \cos\chi e^{-i\psi}|R\rangle + \sin\chi e^{i\psi}|L\rangle, \tag{5}$$

where χ is related to the ellipticity of the beam and ψ is the orientation of the polarization ellipse. Similarly, we can construct the orthogonal state:

$$|e^{\perp}\rangle = -\sin\chi e^{-i\psi}|R\rangle + \cos\chi e^{i\psi}|L\rangle. \tag{6}$$

4
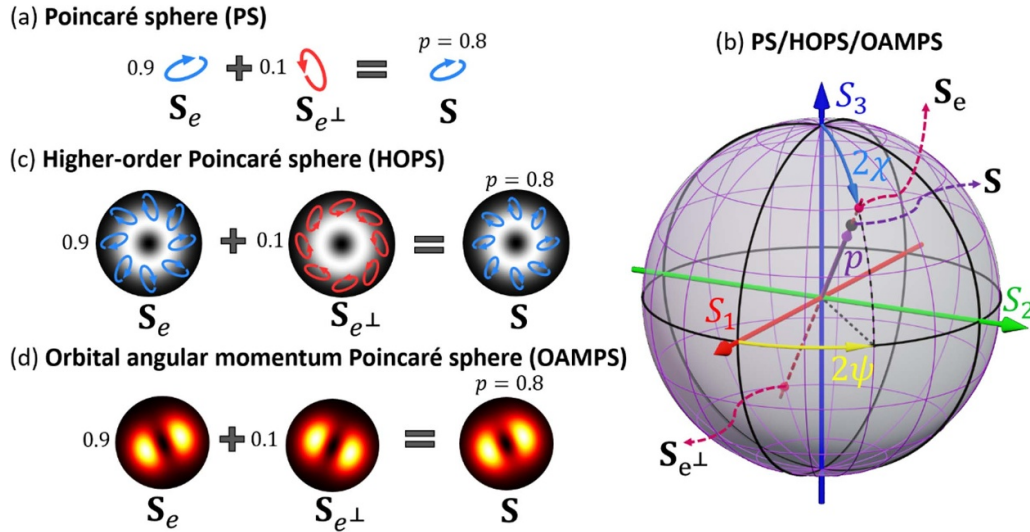
Figure 2. (a) Incoherent superposition of two spatially uniform fully polarized beams with normalized intensities 0.9 and 0.1. (b) Point inside a Poincaré sphere representing a light beam described by the Stokes vector **S** obtained as the incoherent superposition of two beams described by the Stokes vectors $\mathbf{S}_e$ and $\mathbf{S}_{e\perp}$ on the surface of the sphere. Equivalent superposition of (c) two fully polarized vector beams and (d) scalar first-order Gaussian spatial modes. Figure (b) can be regarded as the (a) standard polarization PS, (c) HOPS or (d) OAMPS. The polarization ellipses corresponding to partially polarized light in (a) and (c) describe the polarized part of the state, and they have been rescaled with the DoP.

The Stokes parameters S_i of the pure state $|e\rangle$ are the expectation values $\langle e|\boldsymbol{\sigma}_i|e\rangle$ of the identity operator and the Pauli operators

$$
\begin{aligned}
\boldsymbol{\sigma}_0 &= \boldsymbol{I} = |R\rangle\langle R| + |L\rangle\langle L|, \\
\boldsymbol{\sigma}_1 &= |x\rangle\langle x| - |y\rangle\langle y| = |R\rangle\langle L| + |L\rangle\langle R|, \\
\boldsymbol{\sigma}_2 &= |d\rangle\langle d| - |a\rangle\langle a| = -i|R\rangle\langle L| + i|L\rangle\langle R|, \\
\boldsymbol{\sigma}_3 &= |R\rangle\langle R| - |L\rangle\langle L|,
\end{aligned}
\tag{7}
$$

where $|x\rangle$, $|y\rangle$, $|d\rangle$ and $|a\rangle$ describe linearly polarized light ($\chi = \pi/4$ in equation (5)) with orientation $\psi = 0$, $\pi/2$, $\pi/4$ and $3\pi/4$, i.e. horizontal, vertical, diagonal and antidiagonal, respectively. The Stokes parameters for a mixed state described by ρ_P are the expectation values of the operators $\boldsymbol{\sigma}_i$ with respect to the density operator ρ_P. They can be obtained as $S_i = \mathrm{Tr}(\rho_P\boldsymbol{\sigma}_i)$ [41] using equations (3)–(7), and can be arranged as a Stokes vector:

$$
\mathbf{S} = \begin{bmatrix} S_0 \\ S_1 \\ S_2 \\ S_3 \end{bmatrix} = \begin{bmatrix} 1 \\ p\sin 2\chi\cos 2\psi \\ p\sin 2\chi\sin 2\psi \\ p\cos 2\chi \end{bmatrix}.
\tag{8}
$$

The Stokes parameters S_1, S_2 and S_3 are the Cartesian coordinates in the polarization PS, where 2χ, 2ψ and p are the spherical coordinates. Every state describing fully polarized light ($p = 1$) corresponds to a point on the surface of the polarization PS. As depicted in figure 1(a), the circularly polarized states are at the poles of the sphere ($\chi = 0, \pi/2$), along the S_3 axis. Linearly polarized states, i.e. equally-weighted superpositions of the circularly polarized states ($\chi = \pi/4$), lie on the equator. Polarization states $|x\rangle$ and $|y\rangle$ are on the S_1 axis, while $|d\rangle$ and $|a\rangle$ states are on the S_2 axis. The rest of the points

on the sphere describe elliptically polarized light, with right-handed ellipses lying on the north hemisphere and left-handed ellipses on the south hemisphere. Furthermore, two antipodal points describe a pair of orthogonal polarization states. A partially polarized light beam ($p < 1$) is represented as an inner point in the sphere, and unpolarized light ($p = 0$) lies at the center of the sphere.

In analogy with equation (3), it is convenient to decompose the Stokes vector **S** of a mixed state in equation (8) as the sum of two Stokes vectors $\mathbf{S}_e$ and $\mathbf{S}_{e\perp}$ weighted by the DoP:

$$
\mathbf{S} = \frac{1+p}{2}\mathbf{S}_e + \frac{1-p}{2}\mathbf{S}_{e\perp},
\tag{9}
$$

where the S_1, S_2 and S_3 components of $\mathbf{S}_e^T = [1,\ \sin 2\chi\cos 2\psi,\ \sin 2\chi\sin 2\psi,\ \cos 2\chi]$ and $\mathbf{S}_{e\perp}^T = [1,\ -\sin 2\chi\cos 2\psi,\ -\sin 2\chi\sin 2\psi,\ -\cos 2\chi]$ are the Cartesian coordinates of two antipodal points on the surface of the PS, i.e. two fully polarized orthogonal states. Equation (9) writes **S** as the incoherent superposition of two fully polarized orthogonal beams where the intensity of each beam is weighted by p, as depicted in figure 2(a) for the incoherent superposition of two elliptical fully polarized states. From equations (5) and (6), it is straightforward to show that Stokes vectors $\mathbf{S}_e$ and $\mathbf{S}_{e\perp}$ describe the orthogonal states $|e\rangle$ and $|e^\perp\rangle$, respectively. As depicted in figure 2(b), the state described by **S** lies on the straight line that joins the points $\mathbf{S}_e$ and $\mathbf{S}_{e\perp}$. Its position on the line depends on the relative intensity of each polarization component $|e\rangle$ and $|e^\perp\rangle$, which is given by the DoP. For $p = 0$, the state described by **S** is at the midpoint of the line, i.e. at the center of the sphere. Since equations (3) and (9) are equivalent, the Stokes vector in equation (9) can be rewritten in the well-known relation

$$
\mathbf{S} = (1-p)\,\mathbf{S}_{\mathrm{unpolarized}} + p\mathbf{S}_e,
\tag{10}
$$

where $\mathbf{S}^T_{\text{unpolarized}} = [1, 0, 0, 0]$ describes unpolarized light. Therefore, any Stokes vector can be regarded as the weighted summation of an unpolarized ($\mathbf{S}_{\text{unpolarized}}$) and a fully polarized ($\mathbf{S}_e$) part [18].

2.3. Partially polarized vector beams and their representation in the HOPS

We now use the density operator formalism to describe partially polarized vector beams obtained when passing a partially polarized beam through a *q*-plate device. A *q*-plate is essentially a half-wave linear retarder where the orientation of the optical axis continuously follows *q* times the azimuthal coordinate $\theta = \arctan(y/x)$. Consequently, it imparts a spiral phase $\pm 2q\theta$ to a right and left-circularly polarized beam, respectively, and changes the right-circularly polarized light into left-circularly polarized light and vice versa [12].

A polarized beam bearing a spiral wavefront $\ell\theta$ can be described as the tensor product of two kets $|\ell\rangle \otimes |e\rangle$, where $|\ell\rangle$ denotes a spatial mode of $\ell\theta$ spiral phase and $|e\rangle$ denotes the polarization state. The action of a *q*-plate device $\mathbf{Q}$ of $q = 1/2$ over right and left-circularly polarized states with zero OAM can then be expressed as:

$$\begin{aligned} \mathbf{Q}\,|\ell = 0\rangle\,|R\rangle &= |\ell = +1\rangle\,|L\rangle, \\ \mathbf{Q}\,|\ell = 0\rangle\,|L\rangle &= |\ell = -1\rangle\,|R\rangle, \end{aligned} \tag{11}$$

where we omitted the tensor product symbol $\otimes$ for the sake of simplicity.

A state with zero OAM and DoP given by *p* can be written as in equation (3) by considering each polarization state having a spatial modal part (performing the substitutions $|e\rangle \rightarrow |\ell = 0\rangle|e\rangle$ and $|e^\perp\rangle \rightarrow |\ell = 0\rangle|e^\perp\rangle$):

$$\rho_P^{\ell=0} = \rho_P\,|\ell = 0\rangle\langle\ell = 0|. \tag{12}$$

The operator above corresponds to a mixed state in polarization (i.e. in SAM), but a pure state in OAM. The operator describing the action of the *q*-plate on such a beam can be obtained as:

$$\begin{aligned} \rho_{\text{VB}} = \mathbf{Q}\rho_P^{\ell=0}\mathbf{Q}^\dagger &= \frac{1+p}{2}\Big|e_{\text{VB}}\Big\rangle\Big\langle e_{\text{VB}}\Big| + \frac{1-p}{2}\Big|e_{\text{VB}}^\perp\Big\rangle\Big\langle e_{\text{VB}}^\perp\Big|, \\ \Big|e_{\text{VB}}\Big\rangle &= \cos\chi' e^{-i\psi'}\,|\ell = -1\rangle\,|R\rangle + \sin\chi' e^{i\psi'}\,|\ell = +1\rangle\,|L\rangle, \\ \Big|e_{\text{VB}}^\perp\Big\rangle &= -\sin\chi' e^{-i\psi'}\,|\ell = -1\rangle\,|R\rangle + \cos\chi' e^{i\psi'}\,|\ell = +1\rangle\,|L\rangle, \end{aligned} \tag{13}$$

with $\psi' = -\psi$ and $\chi' = \pi/2 - \chi$. Note that the angles ψ and χ are the same angles controlling the orientation and ellipticity of the polarization ellipse for the input polarization state $|e\rangle$ introduced in equation (5). The operator ρ_{VB} is a mixed state of two orthogonal states $|e_{\text{VB}}\rangle$ and $|e_{\text{VB}}^\perp\rangle$, where the spatial modal part of the beam is non-separable from the polarization content, i.e. they are vector beams [2]. Analogously to equation (3), parameter *p* controls the weight of the $|e_{\text{VB}}\rangle$ and $|e_{\text{VB}}^\perp\rangle$ components in the mixture.

Let us next consider a paradigmatic example of beams carrying OAM: Laguerre–Gaussian beams. A Laguerre–Gaussian beam with zero radial order and azimuthal number $\ell = \pm 1$ is expressed at the waist ($z = 0$) as

$$LG_0^{\pm 1}(r, \theta) = \frac{2r}{\sqrt{\pi}\omega_0^2} e^{-r^2/\omega_0^2} e^{\pm i\theta}, \tag{14}$$

where *r* is the radial coordinate, θ is the azimuthal coordinate, ω_0 is the beam waist, the real exponential is the Gaussian envelope and the complex exponential is the spiral phase.

For an input Gaussian beam LG_0^0 to the *q*-plate, the $|\ell = \pm 1\rangle$ kets in the expressions of $|e_{\text{VB}}\rangle$ and $|e_{\text{VB}}^\perp\rangle$ can be approximated in the far field as Laguerre–Gaussian modes: $|\ell = \pm 1\rangle \rightarrow LG_0^{\pm 1}$ [15]. The beam irradiance profile can be obtained by multiplying the trace of ρ_{VB} by the total beam power *P*. We refer to the trace of ρ_{VB} itself as the intensity profile of the beam $I(r) = \text{Tr}(\rho_{\text{VB}})$:

$$I(r) = \frac{4r^2}{\pi\omega_0^4} e^{-2r^2/\omega_0^2}, \tag{15}$$

where the r^2-dependence indicates a ring-shaped profile. Note that the intensity profile is the same for any input polarization state to the *q*-plate, since it does not depend on the parameters χ, ψ and *p* of the input beam.

On the other hand, the spiral phases in equation (14) account for the spatially-variant polarization patterns of the beams $|e_{\text{VB}}\rangle$ and $|e_{\text{VB}}^\perp\rangle$, where the orientation of the polarization ellipse varies proportional to the azimuthal coordinate θ. For $|e_{\text{VB}}\rangle$, the orientation angle of the polarization ellipse at $\theta = 0$ is ψ', and the beam ellipticity, χ', remains constant along all its transverse section.

Analogously to equations (3) and (13) describes an incoherent superposition of two beams $|e_{\text{VB}}\rangle$ and $|e_{\text{VB}}^\perp\rangle$, which now exhibit spatially-variant polarization patterns (vector beams). The quantity *p* gives the weight of each vector beam in this incoherent superposition. Since both beams have the same intensity profile (equation (15)), they remain superimposed, and therefore the DoP of the resulting vector beam is constant across its transverse section and it is directly given by *p* (the DoP of the input beam).

The HOPS that describes vector beams was defined by Milione *et al* [21]. The radius and the Cartesian coordinates in the HOPS build a new set of Stokes parameters obtained as $S_i = \text{Tr}(\rho_{\text{VB}}\sigma_i')$. Namely, as the expected values in the density operator ρ_{VB} of a version of the identity and the Pauli operators in equation (7)) now expressed in the basis of the direct products $|\ell = -1\rangle\,|R\rangle$ and $|\ell = +1\rangle\,|L\rangle$. Therefore, these new identity and Pauli spin operators (σ_i') can be obtained by substituting the kets $|R\rangle \rightarrow |\ell = -1\rangle\,|R\rangle$ and $|L\rangle \rightarrow |\ell = +1\rangle\,|L\rangle$ and their equivalent bras in equation (7). The Stokes parameters in the HOPS are the same as the ones for the Stokes vector in equation (8) upon substituting $\psi \rightarrow \psi'$ and $\chi \rightarrow \chi'$: $\mathbf{S}^T = [1, p\sin 2\chi' \cos 2\psi', p\sin 2\chi' \sin 2\psi', p\cos 2\chi']$. This resulting Stokes vector can be expressed also as a function of the polarization parameters of the input beam ψ and χ (where $\psi' = -\psi$ and $\chi' = \pi/2 - \chi$) as: $\mathbf{S}^T = [1, p\sin 2\chi \cos 2\psi, -p\sin 2\chi \sin 2\psi, -p\cos 2\chi]$. Note that the position of a point in the HOPS representing a beam traversing the *q*-plate is given by its original position in the PS with an

additional rotation of π radians around the S_1 axis. This is a consequence of the action of a q-plate on the $|R\rangle$ and $|L\rangle$ states described in equation (11), and it is straightforward to understand from the decomposition of a q-plate as the product of a spatially-variant polarization rotator and a half-wave plate [16]. The HOPS Stokes parameters reveal that the one-to-one mapping between the PS and HOPS spheres also includes the inner points.

Figure 1(b) shows the HOPS, with the intensity profile and polarization maps considering first-order LG spatial modes. The circularly polarized LG modes are at the poles, on the S_3 axis. The points on the equator correspond to equally-weighted coherent superpositions of the circularly polarized LG modes with a phase difference of 2ψ, and therefore, their polarization remains linear across its section. Radially polarized and azimuthally polarized beams are paradigmatic examples of vector beams belonging to the equator of the HOPS lying on the S_1 axis. Figure 1 illustrates how a point in the PS with spherical coordinates $(p, 2\chi, 2\psi)$ describing a partially polarized state (figure 1(a)) is mapped, upon traversing a q-plate, onto a point $(p, 2\chi' = \pi - 2\chi, 2\psi' = 2\pi - 2\psi)$ in the HOPS describing a vector beam (figure 1(b)). The inner points in the HOPS are partially polarized vector beams with the same polarization pattern as the totally polarized equivalent vector beam, but with a constant DoP across its transverse section given by p.

The Stokes vector in the HOPS can be decomposed in analogy to the Stokes vector in the PS following equation (9). $\mathbf{S}_e$ and $\mathbf{S}_{e\perp}$ in the decomposition now stand for the fully polarized vector beams $|e_{VB}\rangle$ and $|e_{VB}^\perp\rangle$ in equation (13), and its sum can be regarded as their incoherent superposition. As in the PS, the resulting state in the HOPS lies on the straight line connecting the points described by $\mathbf{S}_e$ and $\mathbf{S}_{e\perp}$ and its position on the line is given by p. Therefore, the center of the sphere ($p = 0$) corresponds to equally-weighted incoherent superpositions of a pair of fully polarized orthogonal vector beams, which are represented as antipodal points on the surface of the HOPS. In addition, the decomposition in equation (10) can also be performed for the Stokes vector in the HOPS, thus regarding a partially polarized vector beam as the superposition of an unpolarized and a fully polarized vector beam.

2.4. Incoherent superposition of first-order spatial Gaussian modes and their representation in the OAMPS

A polarization mixed state described by operator $\boldsymbol{\rho}_P$ in equation (3) can be mapped onto an OAM mixed state upon substituting circular polarization states by OAM states: $|R\rangle \rightarrow |\ell = +1\rangle$ and $|L\rangle \rightarrow |\ell = -1\rangle$. Several approaches have been proposed in the literature for such mapping. A simple approach consists in passing a polarization state through a q-plate followed by a linear polarizer. In this method a fraction of the energy is lost after the polarizer [20]. An alternative method that ideally ensures no energy losses consists in sending the beam exiting the q-plate through an interferometer containing a Dove prism [42]. In this work, the first method is employed for its simplicity, and we normalize the operator describing the resulting state to further obtain the PS-like representation of OAM states with unit radius.

The beam behind the q-plate, which is described by $\boldsymbol{\rho}_{VB}$ in equation (13), is sent through a linear polarizer with horizontal transmission axis, thus described by $\mathbf{P}_x = |x\rangle\langle x|$, where $|x\rangle = (|R\rangle + |L\rangle)/\sqrt{2}$. The normalized resulting beam is given by the following operator:

$$\boldsymbol{\rho}_{OAM}^x = 2\mathbf{P}_x\boldsymbol{\rho}_{VB}\mathbf{P}_x = \rho_{OAM} |x\rangle\langle x| \,, \tag{16}$$

where the modal part is fully contained in the operator ρ_{OAM}:

$$\rho_{OAM} = \frac{1+p}{2}\Big|e_{OAM}\Big\rangle\Big\langle e_{OAM}\Big| + \frac{1-p}{2}\Big|e_{OAM}^\perp\Big\rangle\Big\langle e_{OAM}^\perp\Big|,$$
$$\Big|e_{OAM}\Big\rangle = \cos\chi e^{-i\psi}|\ell = +1\rangle + \sin\chi e^{i\psi}|\ell = -1\rangle \,,$$
$$\Big|e_{OAM}^\perp\Big\rangle = -\sin\chi e^{-i\psi}|\ell = +1\rangle + \cos\chi e^{i\psi}|\ell = -1\rangle. \tag{17}$$

Operator ρ_{OAM} in equation (17) is formally like operator ρ_P for a mixed polarization state (equation (3)) and ρ_{VB} for a mixed vector beam state (equation (13)). Consequently, $\boldsymbol{\rho}_{OAM}$ describes an incoherent superposition of two orthogonal spatial modes $|e_{OAM}$ and $|e_{OAM}^\perp$, which are coherent superpositions of modes with OAM $|\ell = \pm 1\rangle$. The DoP of the initial beam (p) controls the weight of each mode in the incoherent superposition. Operator $\boldsymbol{\rho}_{OAM}^x$ describes a pure state in polarization ($|x\rangle$) but a mixed state of spatial modes, as opposed to operator $\rho_P^{\ell=0}$ in equation (12) that describes the input state to the q-plate consisting on a pure state in spatial modes ($|\ell = 0\rangle$) but a mixed state in polarization.

Once again, a set of OAM Stokes parameters can be obtained as the expected value of the identity operator and the Pauli operators in equation (7) upon substituting $|R\rangle \rightarrow |\ell = +1\rangle$ and $|L\rangle \rightarrow |\ell = -1\rangle$ in ρ_{OAM}. The Stokes parameters are formally like those in equation (8) for the PS, thus defining a point with the same spherical coordinates χ, ψ and p. Therefore, the system q-plate-polarizer maps a point in the PS onto an equivalent point in the OAMPS (figure 1(c)) [20]. Now the poles represent the pure states $|\ell = \pm 1\rangle$ ($p = 1$ and $\chi = 0$, $\pi/2$), which lie on the S_3 axis. Points on the equator are linear combinations of equally-weighted OAM states $(e^{-i\psi}|\ell = +1\rangle + e^{i\psi}|\ell = -1\rangle)/\sqrt{2}$ ($p = 1$ and $\chi = \pi/4$). The OAMPS was first introduced by Padgett and Courtial in [19], where $|\ell = \pm 1\rangle$ were set as Laguerre–Gaussian beams $LG_0^{\pm 1}$. The OAMPS with $LG_0^{\pm 1}$ at the poles is shown in figure 1(c). Note that linear superpositions of $LG_0^{\pm 1}$ with the same amplitude and a phase difference of 2ψ radians result in a first-order HG beam HG_{10} rotated an angle of ψ. The rest of the points on the surface correspond to modes obtained by impinging the q-plate-polarizer system with an input elliptical state. These are pure states described by $|e_{OAM}\rangle$ in equation (17) that can be regarded as coherent superpositions of $LG_0^{\pm 1}$ modes with different weights (χ) and phases (ψ). The OAMPS inner points are mixed states and they represent incoherent superpositions of two orthogonal pure scalar beams $|e_{OAM}\rangle$ and $|e_{OAM}^\perp\rangle$, i.e. located on the surface of the OAMPS. The Stokes vector representing a point inside the OAMPS can also be decomposed using equation (9), where now $\mathbf{S}_e$ and $\mathbf{S}_{e\perp}$ stand for the orthogonal scalar beams in

equation (17). This decomposition reveals that, in analogy to the previous cases in the PS and in the HOPS, a point inside the OAMPS lies on a straight line joining two antipodal points on the surface representing orthogonal states, with its position given by p (figures 2(a) and (d)).

Considering an input LG_0^0 partially polarized beam entering the q-plate-polarizer system, the output beam in the far field can be approximately described by operator ρ_{OAM}^x after substituting $|\ell = \pm 1\rangle \rightarrow LG_0^{\pm 1}$ in equation (17). The trace of ρ_{OAM}^x gives then the intensity of the resulting beam as a function of the polarization parameters χ, ψ and p of the input light:

$$I(r, \theta) = \frac{4r^2}{\pi \omega_0^4} e^{-2r^2/\omega_0^2} \{1 + p \sin 2\chi \cos[2(\theta - \psi)]\}. \quad (18)$$

As for equation (15), the irradiance profile of the beam can be obtained my multiplying $I(r, \theta)$ by the total beam power P. For an input fully polarized linear state ($p = 1, \chi = \pi/4$) equation (18) yields the characteristic double-lobe intensity profile of a HG beam (see figure 1(c)). Interestingly, an analysis of equation (18) reveals that we can find situations where there is not a univocal correspondence between the intensity profile and the modal content of the beam. For example, a totally unpolarized input state ($p = 0$) presents the same ring-shaped intensity profile as a fully polarized circularly polarized beam ($p = 1$ and $\chi = 0$, $\pi/2$). However, according to equation (17), the first case is an incoherent superposition of equally-weighted LG beams, whereas the second case is a pure $LG_0^{\pm 1}$ mode. Also, the intensity profile of an incident elliptically fully polarized state ($p = 1$, $\chi \neq 0, \pi/2, \pi/4$) can as well be achieved by an input partially polarized ($0 < p < 1$) linear or elliptical state, provided the product $p \sin 2\chi$ in equation (18) is kept constant.

Therefore, in these situations it is necessary to retrieve experimentally the modal content of these beams in order to obtain their position in the OAMPS, as will be shown in section 4.

3. Experimental setup

In order to generate any partially polarized state in the PS we propose a new polarization state generator (PSG) shown in figure 3. The main idea is to split two orthogonal polarization components of a randomly polarized laser beam to separately control their relative intensity and then recombine them again. Since these components are uncorrelated, the system performs an incoherent superposition of orthogonal components with different weights, thus creating a mixed state as the one described in equations (3) and (9). Since the state admits a decomposition in its polarized and unpolarized parts, as the one in equations (4) and (10), it is straightforward to see that a linear retarder can be used to control the polarized part of the state, so that any point in the polarization PS can be obtained.

As light source we employed a continuous randomly polarized He–Ne laser of 5 mW and wavelength 543 nm (Melles-Griot 05-LGR-193). These are He–Ne lasers with

internal mirrors attached to the tube, which operate at two orthogonally linearly polarized modes where the orientation of the linear state rapidly changes in time on a nanosecond scale, thus resulting in a light source with random polarization [43]. In all experiments, the laser was left turned on for at least one hour to achieve a stable output. Then, the laser beam was split using a GP linear polarization grating (Edmund Optics #12-677) that adds linear phases of opposite sign to each circular polarization component, thus acting as a circular polarization beam splitter, diffracting the circular components onto the +1 and −1 diffraction orders with a 5° diffraction angle. A converging lens (L1) located at a focal length from the GP grating is used to make these two diffracted beams parallel. A second lens (L2) is placed to join the two beams onto a second GP linear grating (GP2). The 4f system composed of the two lenses (L1 and L2), both with $f = 7.5$ cm focal length, provides imaging of GP1 onto GP2 with minus one magnification. On GP2 the split beams acquire new linear phases that cancel out their original ones. Therefore, the split beams emerge from GP2 recombined and recovering the path prior to the first grating. So far, the described system ideally yields unpolarized light after the second grating, since two uncorrelated circular components with the same intensity were mixed. In order to obtain partially polarized light, the relative amount of each circular component in the incoherent sum was controlled by placing a variable intensity filter in the path of one of the split beams, between lenses L1 and L2. A quarter-wave plate (QWP1), oriented at 45° with respect to the x direction, is placed behind grating GP2 in order to convert the circularly polarized components on each arm into linear states $|x\rangle$ and $|y\rangle$. This way, the incoherent superposition of $|x\rangle$ and $|y\rangle$ states generates a new mixed state along the S_1 axis of the PS, which after traversing the q-plate generates a vector beam along the S_1 axis of the HOPS. This PSG system has several advantages in generating partially polarized light with respect to systems that employ beam-splitters to incoherently mix two laser beams. Namely, higher efficiency in terms of intensity budget, the fact that it is an in-line system, and the easiness in the alignment of the two beams in the near and far field, which is relatively easy to achieve by finding the on-axis position of L1 and GP2 that makes the two beams overlap along the optical path. Furthermore, higher efficiency could be achieved by using Wollaston prisms instead of GP gratings, since they do not exhibit diffraction losses.

After the PSG, the beam was spatially filtered and collimated with a lens (L3) of focal length $f = 10$ cm and then impinges onto a liquid-crystal tunable q-plate of $q = 1/2$ from ArcOptix [44] with its retardance set to π. This way it exhibits a full polarization conversion efficiency and generates a pure vector beam, i.e. a beam whose polarization distribution remains invariant upon propagation [45]. The light exiting the q-plate was sent through a lens (L4) of 2 m focal length that focused the beam onto a camera that captures the Fourier Transform of the q-plate plane. We used a lens with such a long focal length to obtain a large scale of the Fourier transform. The vector beams generated by the q-plate were measured with
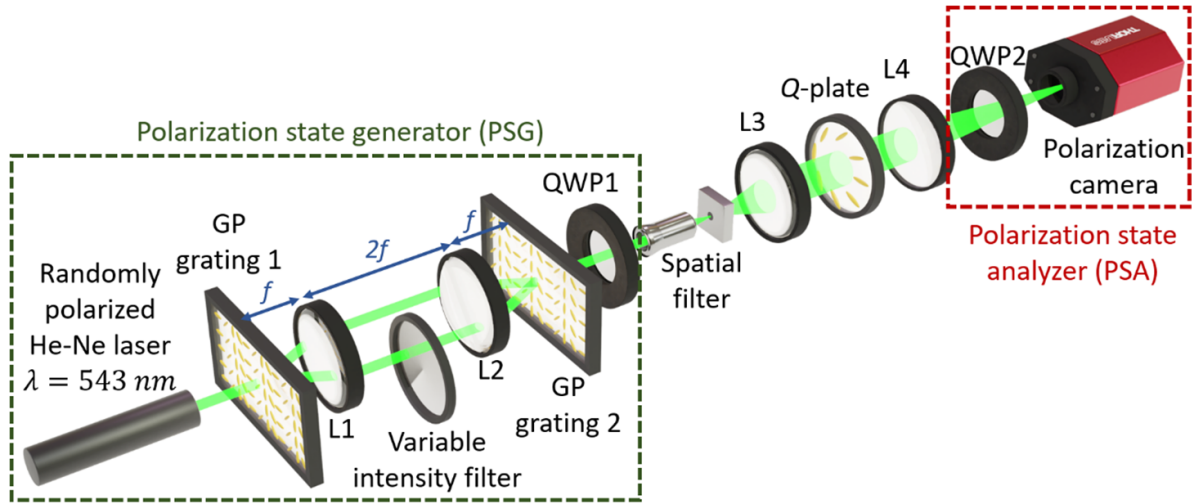
Figure 3. Experimental setup. L (lens), QWP (quarter-wave plate), GP (geometric phase) grating.

a polarization state analyzer (PSA) consisting in a polarization camera (Thorlabs, CS505MUP) and a movable QWP2. The polarization camera consists on pixels of 6.9 μm, where each pixel is made of four micropixels of 3.4 μm, each with a grid polarizer oriented at $0°$, $90°$, $+45°$ and $-45°$, respectively. This PSA is proved to be very useful [46] since it analyzes in a single shot the four linear polarization components and the QWP2 is set before the camera only to measure the circular components. The intensity pattern of the spatial mode in the OAMPS described by equation (18) was obtained as the intensity of the horizontal polarization component, measured by the camera polarizers oriented at $0°$.

In this work, in addition to the polarimetric analysis, we also determine the position in the OAMPS of the modes generated after the q-plate-polarizer system. The equivalent Stokes parameters in the OAMPS of first-order Gaussian modes superpositions can be expressed in terms of the intensities of the HG_{10}, HG_{01}, $HG_{10}(\pi/4)$, $HG_{10}(3\pi/4)$, LG_0^{+1} or LG_0^{-1} components in the beam, analogously to the six classical polarization states measured in Stokes polarimetry [19]: $S_1 = I_{HG_{10}}^{norm} - I_{HG_{01}}^{norm}$, $S_1 = I_{HG_{10}(\pi/4)}^{norm} - I_{HG_{10}(3\pi/4)}^{norm}$ and $S_1 = I_{LG_0^{+1}}^{norm} - I_{LG_0^{-1}}^{norm}$, where the intensities I^{norm} are normalized to the sum of the non-normalized intensities I of any orthogonal pair in the OAM sphere ($I_{HG_{10}} + I_{HG_{01}} = I_{HG_{10}(\pi/4)} + I_{HG_{10}(3\pi/4)} = I_{LG_0^{+1}} + I_{LG_0^{-1}}$).

These intensities are obtained by applying a modal decomposition technique similar to that used in [2]. It is based on the fact that if a given hologram transforms a zero-order Gaussian mode into a high-order mode, then, the inverse hologram will transform the high-order mode into a zero-order Gaussian mode. In this situation, high-intensity values will be detected along the propagation axis. The closer the hologram is to the opposite function of the beam, the higher the intensity at the center will be. Obtaining the Fourier transform of the field amplitude after the hologram provides the correlation between the input beam and the encoded beam. Here, we use holograms with the conjugated phase function of the mode we want to measure. For

simplicity the amplitude information is ignored, since the correlation results show a very good agreement with the expected values.

The holograms are encoded onto a liquid-crystal on silicon SLM (Thorlabs Exulus-HD1 with 1920×1080 pixels of 6.4 μm pixel pitch) placed behind the q-plate. The lens L4, QWP2 and the polarization camera shown in figure 3 were removed. Instead, a horizontal polarizer followed by a linear polarizer oriented at $45°$ and an SLM were placed behind the q-plate. The horizontal polarizer selects the scalar mode described by ρ_{OAM}, the polarizer oriented at $45°$ makes the polarization match the direction of the SLM liquid crystal director. The beam is then sent to the SLM and reflected towards a lens of 1 m focal length that focuses the beam onto a charge-coupled device (CCD) detector. The conjugated phase functions of the modes HG_{10}, HG_{01}, $HG_{10}(\pi/4)$, $HG_{10}(3\pi/4)$, LG_0^{+1} and LG_0^{-1} were sequentially displayed on the SLM. The total intensity I (which is proportional to the measured total power) at the center of the resulting intensity pattern was measured for each hologram within a circle of radius 14 pixels and normalized to the averaged sum of the intensities for the measured orthogonal pairs ($I_{HG_{10}} + I_{HG_{01}} + I_{HG_{10}(\pi/4)} + I_{HG_{10}(3\pi/4)} + I_{LG_0^{+1}} + I_{LG_0^{-1}})/3$. The Stokes parameters in the OAMPS were then obtained with these normalized intensities I^{norm} as explained above. In addition, parameter p in equation (17), which controls the weight of each mode in the incoherent superposition, is obtained as the length of the OAM corresponding Stokes vector and its value is expected to be same as the DoP of the input beam to the q-plate-polarizer system. Note that this value can be regarded as a degree of purity in the equivalent Bloch sphere [36, 37].

4. Results and discussion

We consider three cases: illuminating the q-plate with fully polarized light, with partially polarized light and with unpolarized light. This is achieved by rotating the variable intensity filter in the PSG (figure 3). The experimental
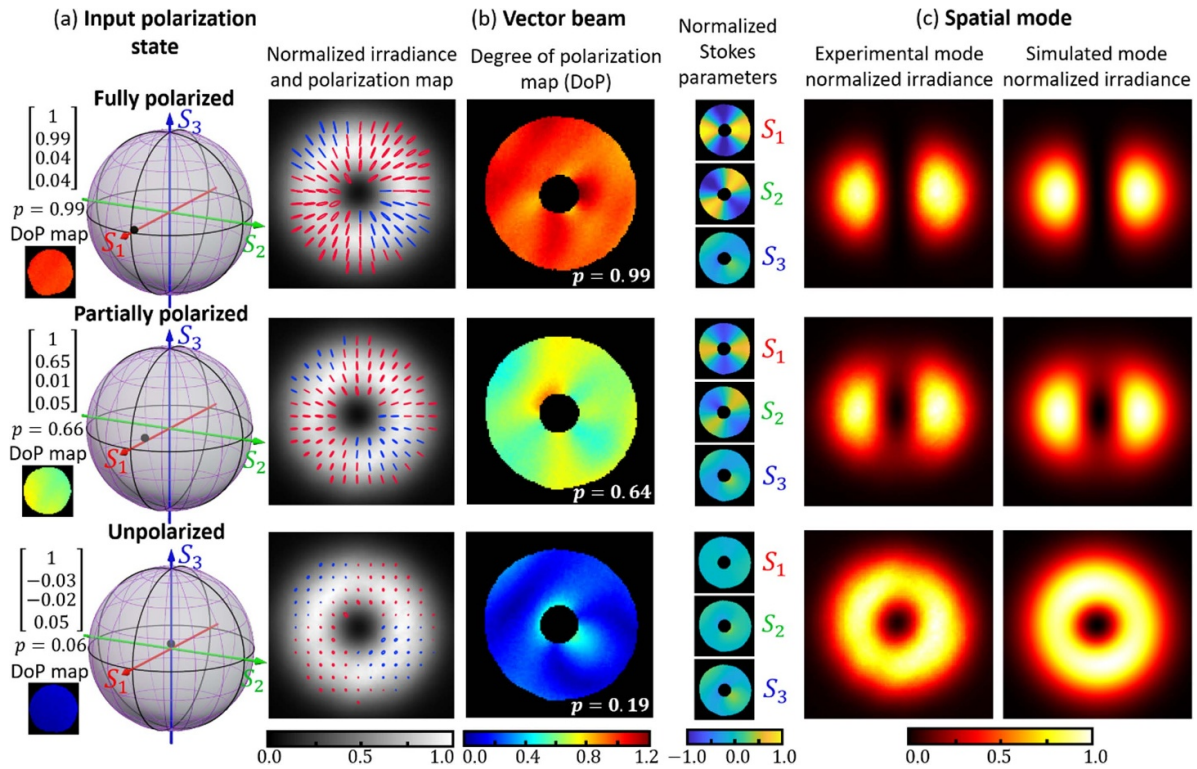
Figure 4. Experimental results. (a) Measured averaged Stokes parameters, DoP map, averaged DoP (*p*) and position in the Poincaré sphere of the state generated in the PSG module of figure 3. (b) Normalized irradiance profile and polarization map, the DoP map, and the normalized Stokes parameters map of the vector beam behind the *q*-plate. The size of each polarization ellipse is rescaled with the value of the corresponding DoP at each point. Right (left)-handed ellipses are plotted in blue (red). (c) Experimental and simulated normalized irradiance of the spatial mode obtained after impinging the vector beam onto a horizontal polarizer.

results for each case correspond to a row in figure 4. Figure 4(a) shows the characterization of the input beam emerging from the PSG having a uniform polarization. These results were obtained setting the tunable *q*-plate at 2π retardance (thus not doing any action), so they can be compared with the results when the *q*-plate is tuned to π retardance. The measured averaged Stokes vector, the DoP map, the averaged DoP (*p*) and the position in the standard PS of the polarization state generated in the PSG are shown in figure 4(a) for each case. The values were computed by averaging the Stokes parameters obtained for each macro-pixel of the camera in the PSA. We only considered for the calculation the points that had a total intensity value greater than 40% of the highest measured value, and these are plotted in the spatial DoP map in figure 4(a). The results show that we are indeed successfully generating three different situations: in the first row the input beam is fully polarized, obtained by fully blocking with the variable intensity filter one of the two beams in the PSG system; the middle row shows a partially polarized state, obtained when the intensity filter allows some light to pass through; and finally, the third row displays the situation where the input beam remains unpolarized, obtained when the beam passing through the intensity filter has the same intensity as the other beam. DoP values $p = 0.99$, 0.66 and 0.06 were experimentally measured for each case.

Figure 4(b) shows the normalized irradiance profile and the polarization map, the DoP map, and the normalized Stokes

parameters map of the vector beam measured after the *q*-plate, now tuned at π retardance to achieve a full efficiency conversion onto a vector beam. Note that the irradiance profile of the vector beam is always ring shaped, as predicted by equation (15). The polarization map and the spatial DoP in figure 4(b) were plotted only at points where the intensity of the beam is above 40% of the highest intensity value. This threshold was used to avoid regions with low irradiance, both at the outer and inner regions, which give rise to non-enough reliable DoP values. Note that despite this relatively high threshold, we are still considering more than 79% of the total beam power.

Each ellipse in the polarization map corresponds to the fully polarized part of the beam at that point, which is described by $\mathbf{S}_e$ in equation (10). Right and left-handed ellipses are plotted in blue and red, respectively. The ellipses were rescaled with the spatial DoP, where larger ellipses mean a higher DoP value at that point. Finally, figure 4(c) shows the normalized irradiance profile obtained when this vector beam is projected on a linear polarizer oriented horizontally. The experimental image is compared with the numerical result in each case. The simulated normalized irradiance profiles were calculated using equation (18) for the values of χ, ψ and *p* obtained from the measured averaged Stokes vector in figure 4(a).

As mentioned before, the first row in figure 4 corresponds to an input fully polarized beam obtained by blocking one of the two beams between lenses L1 and L2 in the

PSG. Consequently, a circularly polarized state emerges from the second GP grating and is transformed into a fully polarized linear state $|x\rangle$ after QWP1. Therefore, the operator describing the vector beam ρ_{VB} in equation (13) stands for a pure state with $p = 1$, $\chi' = \pi/4$ and $\psi' = 0$. The coordinates in the HOPS are expected to be the same as those of the input polarization state in the PS, thus being a radially polarized vector beam, which can be appreciated in the polarization map in figure 4(b). The vector beam's DoP map is near to 1 at every point, as figure 4(b) shows, with an average value of 0.99 that matched the input DoP. On the other hand, considering that the initial state is $|x\rangle$, the spatial mode obtained after the horizontal polarizer behind the q-plate is a pure modal state described by equation (17) with $p = 1$, $\chi = \pi/4$ and $\psi = 0$. Therefore, the irradiance profile of this spatial mode should present the shape of HG_{10}, as expected from equation (18). The simulated normalized irradiance profile in figure 4(c) was actually computed using the measured values of the input polarization state in figure 4(a), and the deviations with respect to the HG_{10} mode are negligible.

The results in the second row in figure 4 were obtained for an input partially polarized beam, where the polarized part of the beam is the same as in the previous case. This state was achieved by reducing the intensity in one of the arms between L1 and L2 by means of a variable intensity filter so that the main arm has the 83% of the total energy. Therefore, the averaged DoP of the input state was found to be $p = 0.66$. The input polarization state is then an incoherent superposition of $|x\rangle$ and $|y\rangle$ states with 0.83 and 0.17 intensities, respectively. Therefore, the resulting vector beam is expected to be a mixed state obtained as the incoherent superposition of a radially polarized vector beam and an azimuthally polarized vector beam with 0.83 and 0.17 normalized intensities, described by the operator ρ_{VB} in equation (13) with $p = 0.66$, $\chi' = \pi/4$ and $\psi' = 0$. The coordinates of the vector beam in the HOPS resulting from this ideal case are expected to match those of the polarization state in the PS: ($S_1 = 0.66, S_2 = 0, S_3 = 0$), which describes a partially polarized radial state. Experimentally, the input Stokes vector was measured to have small values of S_2 and S_3, as shown in figure 4(a). The polarization map in figure 4(b) depicts the measured polarization ellipses of the polarized part of the beam. The map shows the same radial pattern as the fully polarized case does, but we rescaled the size of the ellipses by the DoP value at each point. The averaged spatial DoP of the vector beam was found to be $p = 0.64$, which is close to the expected value $p = 0.66$. Nevertheless, note that the q-plate introduces small modifications in the spatial DoP. This could be ascribed to surface imperfections that affect the spatial homogeneity of the retardance [44]. On the other hand, assuming an input incoherent superposition of $|x\rangle$ and $|y\rangle$ states with 0.83 and 0.17 intensities, the matrix ρ_{OAM} in equation (17), describing the mode after the horizontal polarizer, represents a mixed state of spatial modes with parameters $p = 0.66$, $\chi = \pi/4$ and $\psi = 0$. This is basically an incoherent superposition of modes HG_{10} and HG_{01} with 83% and 17% of the energy, respectively. The simulated and experimental mode normalized irradiance were found very similar;

they both present the two-lobe characteristic structure of HG_{10} but with decreasing lobe, as expected from equation (18).

Finally, the case for input unpolarized light is shown in the third row in figure 4. Unpolarized light was obtained by removing the variable intensity filter between L1 and L2, and thus an equally-weighted incoherent superposition of linearly polarized states $|x\rangle$ and $|y\rangle$ was obtained in the PSG after QWP1. For an input ideal equi-intense superposition of $|x\rangle$ and $|y\rangle$, the vector beam described by ρ_{VB} in equation (13) is a maximally mixed state that can be regarded as an equally-weighted incoherent superposition of a radially polarized beam and an azimuthally polarized beam ($p = 0$, $\chi = \pi/4$ and $\psi = 0$), which results in an unpolarized doughnut-shaped beam. The state is ideally expected to be at the center of the HOPS, as the input state was in the PS. However, as figure 4(b) shows, the q-plate introduces a significant variation in the DoP at several points. Specifically, the averaged DoP of the initial input polarization state (measured with the q-plate tuned at 2π) was found to be $p = 0.06$, while the averaged DoP for the vector beam (with the q-plate tuned at π) is $p = 0.19$. Also note that the ellipses in the polarization map of the obtained vector beam (figure 4(b)) are almost invisible, since the beam was measured as almost unpolarized at every point. With regard to the mode after the polarizer, it should be ideally described by a maximally mixed state that can be considered as the incoherent superposition of two HG modes HG_{10} and HG_{01} with the same intensity ($p = 0$, $\chi = \pi/4$ and $\psi = 0$ for ρ_{OAM} in equation (17)), so it lies at the center of the OAMPS and presents a doughnut-shaped intensity profile. The simulated irradiance profile of the resulting incoherent superposition of modes in figure 4(c) was obtained upon substituting in equation (18) the measured Stokes parameters of the input state in figure 4(a). It presents a doughnut-shaped profile, as the experimentally measured intensity.

Lastly, we illustrate and measure the position in the OAMPS of the spatial modes obtained behind the horizontal polarizer, as shown in figure 4(c). The position in the OAMPS was obtained by measuring with the SLM the modal content of each beam following the procedure explained in the last paragraph of the previous section. Figure 5 shows the normalized irradiance patterns obtained for the three cases with different input after applying six phase masks to the SLM. The masks are displayed in the first row, and they are the conjugate phase of the modes HG_{10}, HG_{01}, $HG_{10}(\pi/4)$, $HG_{10}(3\pi/4)$, LG_0^{+1} and LG_0^{-1}, respectively. The first column shows the irradiance pattern when no phase mask is addressed to the SLM, and they are the same patterns as in figure 4(c). The other images show the corresponding patterns captured at the camera when the phase masks are addressed to the SLM. The normalized irradiance in the center of the pattern provides a measurement of the modal content. For instance, the images in the first row, where a HG_{10} beam is analyzed, provides a bright spot for the binary phase pattern with left/right phase levels, while it is zero when the binary phase pattern is oriented up/down, thus providing a maximum value of the S_1 parameter of the OAMPS. The other four phase masks provide a similar value on the center of the pattern, thus yielding values close to zero for the S_2 and S_3
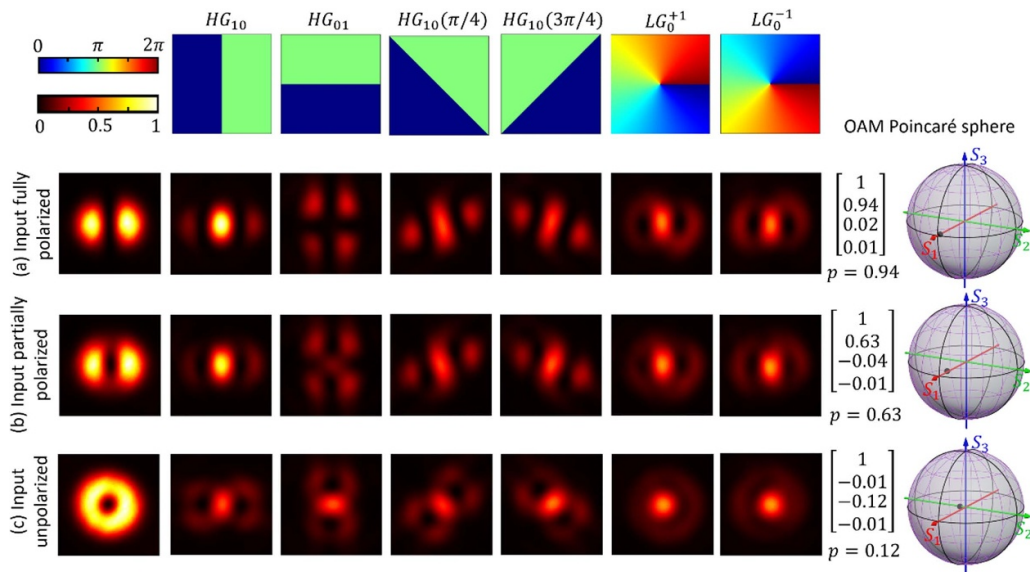
Figure 5. Normalized irradiance patterns measured for six different phase masks applied to the SLM corresponding to the conjugate phase of the modes HG_{10}, HG_{01}, $HG_{10}(\pi/4)$, $HG_{10}(3\pi/4)$, LG_0^{+1} and LG_0^{-1}, respectively. Results for an input beam to the q-plate-polarizer system: (a) fully polarized, (b) partially polarized and (c) unpolarized.

parameters, leading to a successful identification of the HG_{10} mode.

The results in the second and third rows in figure 5, for a partially polarized and for unpolarized input beams, reveal how the bright spot when the HG_{10} mode is detected is progressively reduced, while the irradiance at the center when the HG_{01} mode is detected (which is zero for the fully polarized input beam) progressively increases. The column in the right shows the experimental measures of the OAM equivalent Stokes parameters and the corresponding p values for the three cases, as well as the representation of the mode in the OAMPS. In every case we obtain a very good agreement with the corresponding values in the standard polarization PS for the input beam, except for the somewhat high value of $S_2 = 0.12$ for the unpolarized input beam. This deviation is due to the shape of the doughnut, which resembles the shape of a $HG_{10}(3\pi/4)$, and might be caused by imperfections on the q-plate.

As a final note, let us remark the physical meaning of p in the OAMPS. The light beam analyzed with the modal decomposition is fully polarized in a linear state, since it is measured after the final horizontal polarizer. Therefore, p does not have the physical meaning in terms of the classical DoP as it does in the polarization PS and even in the HOPS. In the OAMPS, it corresponds to the modulus of the Bloch vector that represents the mixed state in the equivalent two-dimensional Bloch sphere [36].

5. Conclusions

In summary, in this work we present a study of how the concept of partial polarization can be extended to vector beams and to OAM modes. The incoherent superposition of polarization states is extended by analogy to superposition of vector beams and the superposition of OAM modes. We apply the density matrix formalism to provide a comprehensive description of the mapping between the classical polarization PS and the HOPS that describes vector beams and the OAMPS that describes OAM modes. As a result, we extend the classical concept of DoP to these other PSs.

Based on this formalism, we analyze the performance of a q-plate device to generate vector beams when being illuminated with a partially polarized input beam. We show that the DoP of the input beam is maintained on the output vector beam. Then, we extend the analysis to the situation where this vector beam is projected onto a linear polarizer to generate a scalar OAM mode. The DoP of the input state p, which is the length of the Stokes vector in the PS representation, is also the length of the equivalent Stokes vectors in the HOPS and in the OAMPS describing the beam after the q-plate and after the polarizer, respectively. While the parameter p controls the DoP of the beam for the PS and for the HOPS, we showed that, in the OAMPS, it weights the incoherent superposition of two modes located on the surface of the sphere. Although we use a simple transmission of the input beam through the q-plate and through a polarizer to transit from the PS to HOPS and to OAMPS, the DoP concept in the PS and in the HOPS and its equivalent parameter in the OAMPS are applicable to other procedures of generating vector beams and OAM modes.

In order to experimentally verify the results, we propose a new experimental PSG arrangement to generate an input beam with partial polarization, where the DoP can be controlled. Using a randomly polarized laser as light source, we build an optical system using GP gratings to split and recombine the input beam. By setting the relative intensity between the two split beams, the DoP of the recombined beam can be easily and efficiently controlled. The beam emerging from this PSG then illuminates a tunable q-plate device. The generated

output vector beam is analyzed in terms of the polarization state, and the scalar mode obtained upon projecting onto a linear polarizer is analyzed in terms of the modal decomposition. The experimental results show a very good agreement with the expected values and demonstrate that the characterization of the p parameter can be performed in each PS domain, and that it preserves its value in the mapping process.

Data availability statement

The data that support the findings of this study are available upon reasonable request from the authors.

ORCID iDs

David Marco https://orcid.org/0000-0003-0039-4161
María Del Mar Sánchez-López https://orcid.org/0000-0002-6286-0079
Carlos Hernández-García https://orcid.org/0000-0002-6153-2647
Ignacio Moreno https://orcid.org/0000-0002-1550-0601

References

[1] Pachava S, Dharmavarapu R, Vijayakumar A, Jayakumar S, Manthalkar A, Dixit A, Viswanathan N K, Srinivasan B and Bhattacharya S 2019 Generation and decomposition of scalar and vector modes carrying orbital angular momentum: a review *Opt. Eng., Bellingham* **59** 041205
[2] Rosales-Guzmán C, Ndagano B and Forbes A 2018 A review of complex vector light fields and their applications *J. Opt.* **20** 123001
[3] Rubinsztein-Dunlop H *et al* 2017 Roadmap on structured light *J. Opt.* **19** 013001
[4] Ritsch-Marte M 2017 Orbital angular momentum light in microscopy *Phil. Trans. R. Soc.* A **375** 20150437
[5] Jin Y, Allegre J, Perrie W, Abrams K, Ouyang J, Fearon E, Edwardson S P and Dearden G 2013 Dynamic modulation of spatially structured polarization fields for real-time control of ultrafast laser-material interactions *Opt. Express* **21** 25333–43
[6] Jesacher A, Furhapter S, Bernet S and Ritsch-Marte M 2004 Size selective trapping with optical "cogwheel" tweezers *Opt. Express* **12** 4129–35
[7] Willner A E *et al* 2015 Optical communications using orbital angular momentum beams *Adv. Opt. Photonics* **7** 66–106

[8] Goyal S K, Roux F S, Forbes A and Konrad T 2013 Implementing quantum walks using orbital angular momentum of classical light *Phys. Rev. Lett.* **110** 263602
[9] Beijersbergen M W, Allen L, Van der Veen H E L O and Woerdman J P 1993 Astigmatic laser mode converters and transfer of orbital angular momentum *Opt. Commun.* **96** 123–32
[10] Carpentier A V, Michinel H, Salgueiro J R and Olivieri D 2008 Making optical vortices with computer-generated holograms *Am. J. Phys.* **76** 916–21
[11] Curtis J E and Grier D G 2003 Structure of optical vortices *Phys. Rev. Lett.* **90** 133901
[12] Marrucci L, Manzo C and Paparo D 2006 Optical spin-to-orbital angular momentum conversion in inhomogeneous anisotropic media *Phys. Rev. Lett.* **96** 163905
[13] Rubano A, Cardano F, Piccirillo B and Marrucci L 2019 Q-plate technology: a progress review *J. Opt. Soc. Am.* B **36** D70–D87
[14] Beresna M, Gecevičius M, Kazansky P G and Gertus T 2011 Radially polarized optical vortex converter created by femtosecond laser nanostructuring of glass *Appl. Phys. Lett.* **98** 201101
[15] Cardano F, Karimi E, Marrucci L, de Lisio C and Santamato E 2013 Generation and dynamics of optical beams with polarization singularities *Opt. Express* **21** 8815–20
[16] Davis J A, Hashimoto N, Kurihara M, Hurtado E, Pierce M, Sánchez-López M M, Badham K and Moreno I 2015 Analysis of a segmented *q*-plate tunable retarder for the generation of first-order vector beams *Appl. Opt.* **54** 9583–90
[17] McLaren M, Konrad T and Forbes A 2015 Measuring the nonseparability of vector vortex beams *Phys. Rev.* A **92** 023833
[18] Goldstein D H 2010 *Polarized Light* (New York: Marcel Dekker)
[19] Padgett M J and Courtial J 1999 Poincaré-sphere equivalent for light beams containing orbital angular momentum *Opt. Lett.* **24** 430–2
[20] Marrucci L, Karimi E, Slussarenko S, Piccirillo B, Santamato E, Nagali E and Sciarrino F 2012 Spin-to-orbital optical angular momentum conversion in liquid crystal "q-plates": classical and quantum applications *Mol. Cryst. Liq. Cryst.* **561** 48–56
[21] Milione G, Sztul H I, Nolan D A and Alfano R R 2011 Higher-order Poincaré sphere, stokes parameters, and the angular momentum of light *Phys. Rev. Lett.* **107** 053601
[22] Yi X, Liu Y, Ling X, Zhou X, Ke Y, Luo H, Wen S and Fan D 2015 Hybrid-order Poincaré sphere *Phys. Rev.* A **91** 023801
[23] Chen S, Zhou X, Liu Y, Ling X, Luo H and Wen S 2014 Generation of arbitrary cylindrical vector beams on the higher order Poincaré sphere *Opt. Lett.* **39** 5274–6
[24] Gálvez E J, Khadka S, Schubert W H and Nomoto S 2012 Poincaré-beam patterns produced by nonseparable superpositions of Laguerre-Gauss and polarization modes of light *Appl. Opt.* **51** 2925–34
[25] Van Eeckhout A, Garcia-Caurel E, Ossikovski R, Lizana A, Rodríguez C, González-Arnay E and Campos J 2020 Depolarization metric spaces for biological tissues classification *J. Biophoton.* **13** e202000083
[26] He C, He H, Chang J, Chen B, Ma H and Booth M J 2021 Polarisation optics for biomedical and clinical applications: a review *Light Sci. Appl.* **10** 194
[27] Angelo J P, Germer T A and Litorja M 2019 Structured illumination Mueller matrix imaging *Biomed. Opt. Express* **10** 2861–8

[28] Suárez-Bermejo J C, González de Sande J C, Santasiero M and Piquero G 2019 Mueller matrix polarimetry using full Poincaré beams *Opt. Lasers Eng.* **122** 134–41

[29] Barreau L *et al* 2018 Evidence of depolarization and ellipticity of high harmonics driven by ultrashort bichromatic circularly polarized fields *Nat. Commun.* **9** 4727

[30] Zurrón-Cifuentes O, Boyero-García R, Hernández-García C, Picón A and Plaja L 2019 Optical anisotropy of non-perturbative high-order harmonic generation in gapless graphene *Opt. Express* **27** 7776–86

[31] Chang K-Y, Huang L-C, Asaga K, Tsai M-S, Rego L, Huang P-C, Mashiko H, Oguri K, Hernández-García C and Chen M-C 2021 High-order nonlinear dipole response characterized by extreme-ultraviolet ellipsometry *Optica* **8** 484–92

[32] Carbajo S, Granados E, Schimpf D, Sell A, Hong K H, Moses J and Kärtner F X 2014 Efficient generation of ultra-intense few-cycle radially polarized laser pulses *Opt. Lett.* **39** 2487–90

[33] Alonso B, Lopez-Quintas I, Holgado W, Drevinskas R, Kazansky P, Hernández-García C and Sola I 2020 Complete spatiotemporal and polarization characterization of ultrafast vector beams *Commun. Phys.* **3** 151

[34] Hernández-García C, Turpin A, San Román J, Picón A, Drevinskas R, Cerkauskaite A, Kazansky P G, Durfee C G and Sola I J 2017 Extreme ultraviolet vector beams driven by infrared lasers *Optica* **4** 520–6

[35] de Las Heras A *et al* 2022 Extreme-ultraviolet vector-vortex beams from high harmonic generation *Optica* **9** 71–79

[36] Gamel O and James D F V 2012 Measures of quantum state purity and classical degree of polarization *Phys. Rev.* A **86** 033830

[37] Gil J J 2020 Sources of asymmetry and the concept of nonregularity of n-dimensional density matrices *Symmetry* **12** 1002

[38] Lizana A, Estévez I, Torres-Ruiz F A, Peinado A, Ramírez C and Campos J 2015 Arbitrary state of polarization with customized degree of polarization generator *Opt. Lett.* **40** 3790–3

[39] Marco D, López-Morales G, Sánchez-López M M, Lizana A, Moreno I and Campos J 2021 Customized depolarization spatial patterns with dynamic retardance functions *Sci. Rep.* **11** 1–13

[40] Wei B Y, Chen P, Ge S J, Zhang L C, Hu W and Lu Y Q 2016 Liquid crystal depolarizer based on photoalignment technology *Photon. Res.* **4** 70–73

[41] Wolf E 2007 *Introduction to the Theory of Coherence and Polarization of Light* (Cambridge: Cambridge University Press)

[42] Karimi E, Slussarenko S, Piccirillo B, Marrucci L and Santamato E 2010 Polarization-controlled evolution of light transverse modes and associated Pancharatnam geometric phase in orbital angular momentum *Phys. Rev.* A **81** 053813

[43] Brand U, Mensing F and Helmcke J 1989 Polarization properties and frequency stabilization of an internal mirror He-Ne laser emitting at 543.5 nm wavelength *Appl. Phys.* B **48** 343–50

[44] ArcOptix Variable spiral plate (VSP) for vortex beam generation (available at: http://arcoptix.com/Q_Plate.htm)

[45] Sánchez-López M M, Davis J A, Moreno I, Cofré A and Cottrell D M 2019 Gouy phase effects on propagation of pure and hybrid vector beams *Opt. Express* **27** 2374–86

[46] López-Morales G, Sánchez-López M M, Lizana Á, Moreno I and Campos J 2020 Mueller matrix polarimetric imaging analysis of optical components for the generation of cylindrical vector beams *Crystals* **10** 1155